Rayleigh-Taylor instability of thin films of granular suspensions: patterns, dynamics, and inhibition

Alice Pelosse, Élisabeth Guazzelli, Matthieu Roché

Rayleigh-Taylor instability of thin films of granular suspensions: patterns, dynamics, and inhibition

Alice Pelosse,[1] Élisabeth Guazzelli,[1] and Matthieu Roché[1,*]

[1]*Université Paris Cité, CNRS UMR 7057, Laboratoire Matière et Systèmes Complexes, Paris, France*

(Dated: January 6, 2025)

The instability of a thin film because of its own weight, commonly named the Rayleigh-Taylor instability, is investigated with density-matched suspensions under various confinement of the particles phase. For small confinement, the instability pattern and the dynamics is accurately described by the prediction obtained with the continuous model using the bulk suspension viscosity. The layer then develops a hexagonal pattern of bumps and the instability propagates as a front usually starting from the outer boundary of the layer. Increasing the confinement i.e. increasing particle size or decreasing the thickness of the fluid layer yields a completley different behaviour of the layer of suspension. The front propagation is not observed, and only a few domes grow and then move across the thin film.

The Rayleigh-Taylor instability (RTI) occurs in accelerated two-phase fluid systems with adverse density gradients, i.e. systems where the denser phase lies on top of the lighter one[1–3]. This instability is observed in many natural systems, e.g. during the collapse of the core of massive stars [4]. It is also believed to play a role in geophysical processes such as diapirism and mantle dynamics [5]. Industrial applications such as coating and inertial confinement fusion may also display the instability, to their benefit to obtain patterned surfaces [6] or disadvantage, destroying the symmetry of the fusion fuel target implosion [7]. Dry and immersed granular materials also display a similar instability [8, 9].

In general, the RTI is hard to prevent. Rotation of the upper liquid [10], horizontal oscillations of the system [11, 12], a tangential flow in the liquid film[13–17], or the presence of a thermocapillary stress at the interface [18] can help mitigate the instability. Prevention of the instability has also been reported for a liquid/liquid interface in a vertically confined system with a suspension of buoyant particles on top [19].

In particular, in the situation of a viscous thin film, a hexagonal pattern of domes is shown to be the fastest growing mode in the linear regime of the instability growth [20].

In a gravity field, these configurations are unstable to any perturbation of their interface in the absence of stabilizing forces [21]. For two immiscible viscous fluids, the competition of stabilizing capillarity and viscosity with gravity leads to the selection of a pattern with wavelength pattern selection and specific dynamics depending on the situation [22, 23].

For a thin liquid film of thickeness h_0, a normal mode analysis shows that this situation is unstable. The instability is characterized by a mode of fastest growth with wavelength λ^* and growth rate τ^* given by [24]

$$\lambda^* = 2\pi\sqrt{2}\ell_c, \quad \tau^* = 12\frac{\eta}{\gamma}\frac{\ell_c^4}{h_0^3}, \tag{1}$$

where g is the gravity acceleration, η, γ and ρ are the viscosity, surface tension with the air and density of the liquid, respectively. We also introduce the capillary length, $\ell_c = (\gamma/\rho g)^{1/2}$.

Real thin films are bounded either by a wall or a contact line.Y a t'il un lien logique entre ces deux phrases? Preciser que c'est une selection de pattern rajouter ta REF Matthieu The study of their RTI of a thin viscous film shows a more complex picture [20, 25, 26]. The disturbance may grow into different patterns depending both on the edge conditions and non-linear couplings between unstable modes. For example, rolls are observed in the first stage of the instability before being superseded by a faster growing hexagonal pattern of domes as the instability progresses [20]. Also, the instability propagates across the film forming a front. While the wavelength of the rolls is close to λ^*, the distance separating two domes is larger due to geometrical arguments. Indeed, the domes grow on the rolls, each row being interspersed in the middle of its two neighbors. As a result, the distance between two domes is $L^* = 2\lambda^*/\sqrt{3}$.

Here, we show that seeding solid particles in a thin film is another way to control its destabilization by the Rayleigh-Taylor mechanism. Using concentrated suspensions of athermal particles, we observe that the dynamics of the instability, i.e. the growth of domes on the film, depends on the ratio of the diameter of the particles, d, to the film thickness, h_0. When $d/h_0 << 1$, the profile is the one expected for a simple fluid of the same viscosity as the suspension. When $d/h_0 >> 1$, the pattern is on average still close to that of the pure-fluid case but shows disorder. The liquid domes move along the film before dripping. During motion, they may coalesce. We characterize the motion of the **domes**, and show that it is related to a similar phenomenon observed and predicted on very thin films. For quantitative discussions on dome motion and growth rate, we use surface profilometry to reconstruct the height profile of the film during the growth of the instability. We also propose a mechanism to explain the observed dynamics.

METTRE EN AVANT QU'ON EST 3D

The dome patterns observed for a 750-µm thick layer of pure fluid and suspensions made with different particle sizes are displayed in Fig. 1 (a). The patterns in the top right and left quadrants, corresponding to a pure fluid film and a suspension film made of 60-µm particles, display a high dome number and a regular hexagonal organization of the domes. In

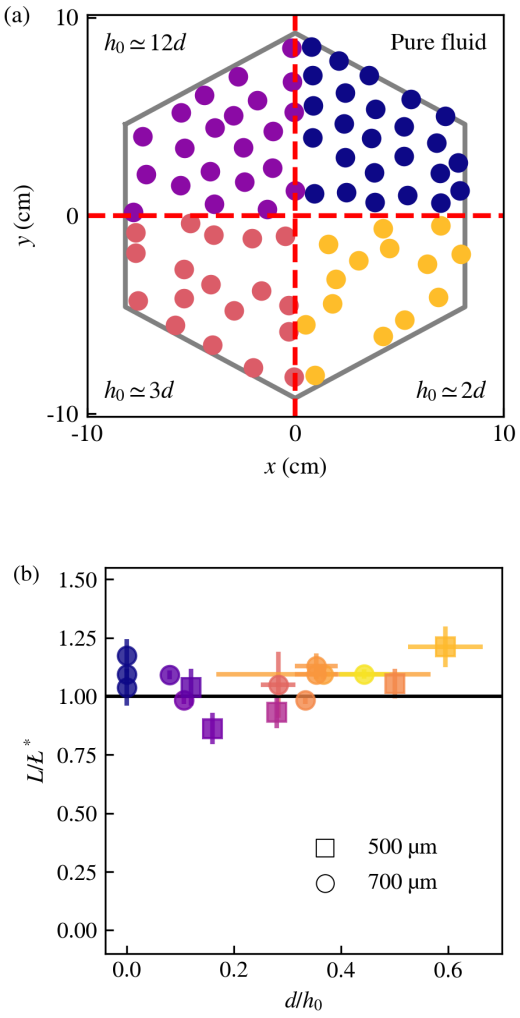

FIG. 1. (a) Dome pattern i.e. dripping locations, for fluid layers of 750 µm made of pure fluid (top right) of granular suspensions of different particle sizes. The suspending fluid is the Triton mixture and and particles are made of PMMA. (b) Position of the first peak of $g(r)$, normalized by the linear prediction of the fastest growing wavelength $L^* = 4\pi\sqrt{2}\ell_c/\sqrt{3}$ for suspensions made with the Triton mixture and PMMA particles and those made with the PEG copolymer and PS particles. Color corresponds to particle size and symbol shape correspond to the initial thickness of the fluid layer.

contrast, much scarcer and less regular patterns are observed for larger particles in the bottom left and right quadrants, for particle sizes of 265 µm and 235 µm, respectively. The pattern selection is thus not affected by the addition of small non-confined particles but breaks down when the film thickness is only a few particle diameters. For the largest particles, we collected drops as they fall and confirmed that their volume fraction is the same as that of the suspension.

From the radial distribution function $G(r)$ of the dome distances, we inferred the mean distance between nearest neighbors L. For a given suspending fluid, we found L to be insensitive to the addition of particle, and also insensitive to their size. For the pure fluid, secondary and tertiary peaks, coming from the high spatial ordering of the lattice, can be observed at larger distances, but these peaks are less pronounced upon the addition of particles. The position of the largest peaks at $r = L$, for different suspensions made with different particle sizes, suspending fluids, and initial thicknesses, is plotted in Fig. 1 (b). In order to remove variations due to fluid properties, this mean distance between domes is normalized by the one expected for the hexagonal pattern, $L^* = 4\pi\sqrt{2}\ell_c/\sqrt{3}$. For all the fluids, pure liquids and suspensions, the normalized radial distance associated with the maximum of $G(r)$, falls on the line $L/L^* = 1$. This agreement with the prediction can be expected. Indeed, as the wavelength of the instability, setting eventually the distance between domes, does not depend on the film thickness, h_0, nor on the liquid viscosity, η, it should not be affected by the addition of the particles. However, for the largest particle, the instability pattern is very different, and the wavelength selection is thus non-trivial.

As mentioned above, the addition of particles should not modify the surface tension compared to the case of pure fluid, but it should increase the dissipation and therefore the effective viscosity of the fluid by a factor $\eta_r = 5$ for $\phi = 30\%$, where η_r is often referred to as the relative viscosity of the suspension [27]. This increase in viscosity does not affect the wavelength of the linear regime, but it should increase the characteristic time of the growth of the instability. The latter can be quantified for transparent suspension as the pattern distortion can be inverted into height to extract growth rates for each dome, fitting dome height by exponential functions. The fitting was performed above 0.5 mm to avoid noise in detection, and below 2 mm that is considered as the typical height above which the Schlieren analysis becomes non-valid [28]. Additionally, a criterion on a minimal dome height of 1 mm ensures to track domes that drip over the course of the experiment. The distribution of growth rates for a film made of pure fluid and suspensions of small and large particles are gathered in Fig. 2. A map of the spatial distribution of the growth rate is also displayed. The grey dots correspond to domes out of which no growth rate could be extracted, due to insufficient height reached by the dome. For pure fluid, the average of the growth rates is $\tau = 80$ s, in the same order of magnitude as that of the prediction from the linear theory, $\tau = 21$ s. The discrepancy could stem from analysis out of the linear regime, where growth rate accelerates, but the agreement remains satisfactory. Upon the addition of small particles, the growth rate distribution widens and shifts toward larger growth rates. The average growth rate, $\tau = 365$ s is almost 5 times higher than that of the pure fluid, suggesting that the linear theory is still valid for this suspension, as the growth rate is expected to be proportional to the fluid viscosity. For the largest particles, the conclusion is less clear, particularly due to the significant number of domes for which an exponential fit is impossible. The average growth rate would be slightly higher than in the case of small particles, $\tau = 391$ s but this conclusion lacks statistics due to the smaller number of domes This difference

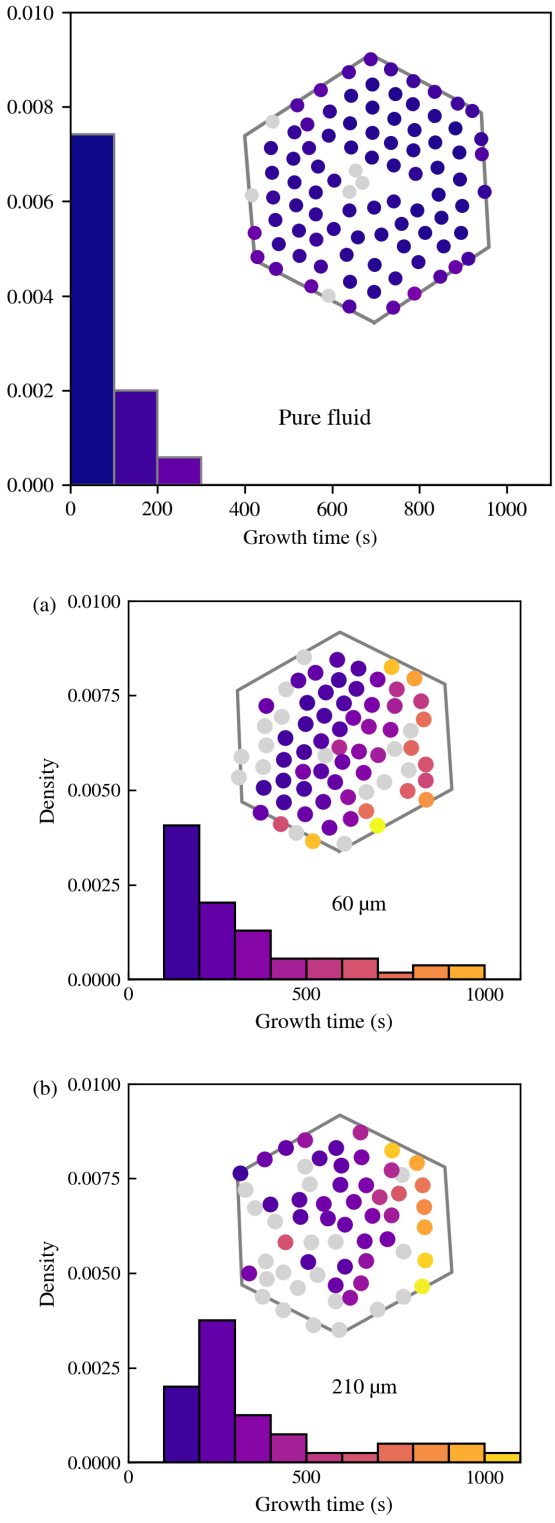

FIG. 2. Dome growth rate distribution (bars) and dripping locations (hexagons) for (a) the mixture of Triton and for suspensions made of 9b) 60-µm PMMA particles and (c) 210-µm PMMA particles. Grey dots correspond to domes for which the height doesn't reach 1 mm.

can be in part explained by a different growth mechanism of the instability, with moving domes, as explained in the following.

As seen in Fig.1 and Fig.2, the dripping positions of the domes for the pure fluid and the suspension with small particles are well-ordered, forming a quasi-hexagonal lattice. In contrast, the suspension containing large particles exhibits a less organized pattern. This reduced order is due to the increased mobility of domes in the suspension with large particles. By linking the dome positions into trajectories using the Python module trackpy, we can extract dome trajectories to evaluate the stability of the pattern, as displayed for various particle sizes in Fig. 3. For both the pure fluid and suspensions with small particles, domes remain stable during a single growth phase, as well as across successive generations of domes, which are highlighted by brighter colors (up to four generations at the same location for the pure fluid). However, for films containing large particles, this stability no longer holds. Dome positions tend to drift during individual trajectories and across subsequent generations of domes. This motion is predominantly directed from the edges towards the center of the film. Importantly, this behavior is not caused by plate tilting, as it is absent in the pure fluid and suspensions with small particles. Furthermore, there is no consistent trend in dome directionality between different experiments.

To quantify dome displacement, the mean square displacement $|\Delta r|$ over $\Delta t = 50\,\mathrm{s}$ for each trajectory has been computed and converted into a mean dome speed $v_m = |\Delta r|/\Delta t$. Density histograms of the mean dome speeds are shown for an experiment with pure fluid and with a suspension made of large particles in the main graph of Fig. 3b. This analysis confirms the earlier observation regarding dome mobility: the mean square displacement or equivalently the mean dome speed of the pure fluid is significantly smaller compared to that of a suspension made of large particles. The excess density of domes at high speed compared to the case of the pure fluid, M (i.e., the area between the two smooth curves) is plotted as a function of particle size in the inset of Fig. 3b. This increase in mobility, relative to the pure fluid, grows almost linearly with particle size.

The behavior of a free interface coupled the mechanics of complex fluid is a tedious problem. In the canonical case of granular suspensions, dip coating [29–32], pinch-off [33, 34] and wetting [35, 36] have revealed that systems behave as regular fluid as long as confinement of the particulate phase remains mild. In this paper, we reach the same conclusion with two distinct regimes, depending on the ratio d/h_0. For small ratios, the confinement on the particles is mild and the suspension behaves like a regular fluid with effective properties to account for the addition of particles. In particular, the increase in dissipation, resulting in a larger viscosity, shows up in the growth rate of the domes. The increase in growth rate is the same as that of viscosity (by a factor $\eta_r = 5$). The wavelength of the instability is not modified as the addition of particles to the fluid does not change the capillary length. The conclusions are different when the confinement of the particles increases; that is, as $d/h_0 \to 1$. In particular, the hexagonal

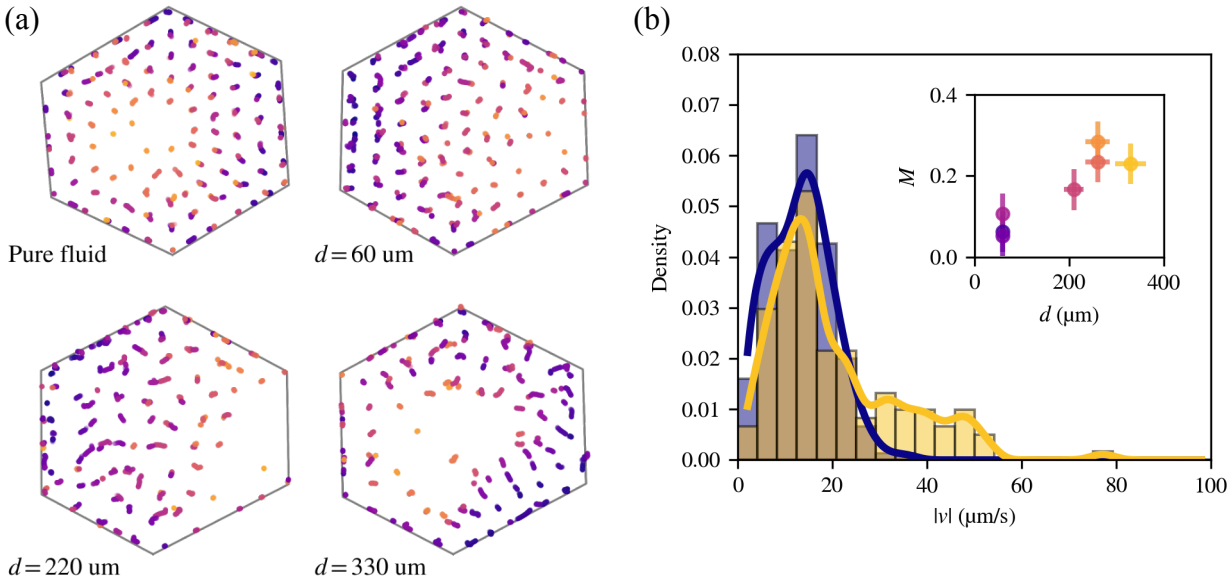

FIG. 3. Dome trajectories. Je propose de merger les deux figures car elles parlent de la même idée. Aussi, ça permet de mettre ton diagramme de fonctionnement en figure 4, qui me semble une très bonne conclusion du papier. Dis moi ce que tu en penses. Il y a l'air d'y avoir un souci avec les hexagones aussi, ils n'ont pas l'air régulier, c'est normal? Dans la figure b, ce serait p-ê bien d'avoir une légende indiquant la taille des particules et la couleur des courbes.

lattice does not form, and we observe a completely different propagation mechanism, with fewer domes invading the films and moving to gather fluid and grow. For pure fluid and small particles, the domes are very stable during one growth event, but also for the next generations of domes. We rationalize this observation by a competition between the growth of the instability and resistance against film thinning, coming from the viscous and capillary forces. When particles are in the fluid, additional forces coming from meniscii on the particles and forbidden rearrangements under confinement reinforce the resistance against film thinning. Assuming this mechanism prevents thinning below the diameter of a single particle, we build a simple model which compares the dripping volume to the available fluid volume per unit cell of the theoretical hexagonal lattice.

As the instability grows, domes become higher and may eventually release a drop above a critical size that can be estimated with the critical volume of a pendent drop in perfect wetting on the upper wall, $V_0^{\max} \sim 6\pi\ell_c^3$ [37–39]. Dripping can however be delayed significantly with extremely thin and/or extremely viscous liquid layers and/or small enough initial perturbation [40]. For the hexagonal pattern with domes spaced by $L^* = 2\lambda^*/\sqrt{3}$, the available fluid volume per unit cell is $V_0 = 16\pi^2\ell_c^2 h_0/\sqrt{3} = Ah_0$ [20]. If only this volume of liquid contributes to dome growth, i.e. there is no drainage of the liquid in neighboring cells, the dripping criterion for this growing dome is $V_0 \geq V_0^{\max} \sim 6\pi\ell_c^3$ yields $h_0 \geq 0.21\ell_c = 360 - 383$ μm in the current experiments for the hexagonal pattern. Introducing particles into the liquid increases this lower bound in film thickness, assuming that some fluid becomes unavailable for dripping because of capillary forces acting on the particles and preventing the draining of the first layer of suspension. If a layer of thickness d is immobilized below the top plate, the modified dripping criterion becomes $V_0 = Ah_0 \geq V_0^{\max} + Ad$ i.e. $d \leq h_0 - 3\sqrt{3}\ell_c/(8\pi) \simeq h_0 - 0.21\ell_c$. For $h_0 = 750\,\mu$m, we reach $d \leq 372 - 395$ μm. This order of magnitude aligns with observations of unstable hexagonal patterns in Figures 1(a) and 3(a). To enable dripping, domes must move out of their cells; otherwise, growth is hindered, as illustrated by the numerous gray dots in the inset of Figure 2(b). More generally, the number of domes decreases with increasing particle size, which is again consistent with the proposed mechanism. The little offset could stem from a dripping volume that is underestimated. Indeed, the prediction $V_0^{\max} \sim 6\pi\ell_c^3$ holds for infinite time. In experiments, other phenomena with finite timescales are involved and can disturb a growing dome if the dripping process is too slow. We measured the dripping limit for isolated drops, as is defined $V_0^{\max}$, for a suspensions of 250-μm particles and found indeed that the minimum volume to observe dripping is larger than the prediction by more then 50 %

This new propagation mechanism of the instability is based on the increased mobility of few domes. As the dome growth is constrained due to the excluded volume effect of the particles, the instability promotes dome motion. Domes then gather fluid on their trajectory, grow and eventually drip. However, this mechanism seems overall less efficient, resulting in fewer dripping events, see Fig.2. The increased mobility of domes in suspensions with larger particles also leads to the coalescence of neighboring domes, which similarly helps overcoming the constraints imposed by the excluded volume near the ceiling. To the best of our knowledge, this sponta-

neous translation of a pending drop on a flat horizontal ceiling has not been reported experimentally in the literature. However, the translation of pendant drops along a flat horizontal ceiling has been predicted and reported in numerical simulations [41]. The mechanism described in these simulations involves an asymmetry in the film thickness, which leads to asymmetric drainage and a preferred migration of a dome to the region with the largest film thickness. In addition, this translation is self-maintained, as the dome creates a shallower trailing wake as it moves. In these simulations, the surrounding film is very thin, such that the volume available for dripping is similarly constrained, as the drainage is very slow. The conditions required for such translational motion to occur appear highly restrictive. Specifically, the film thickness must be very small (by an order of magnitude thinner) compared to the height of the dome. The translation speed is expected to scale with the dome height h_d, and the film thickness h_+ in front of the drop, following the equation:

$$v \simeq 0.00485(h_+ h_d)^{3/2}\left[1+2.04\left(\frac{h_d}{h_+}\right)^{1/2}\right]. \qquad (2)$$

For a moving dome, the film in the trailing wake is extremely thin, such that h_+ is then almost equivalent to the height difference between the front and the rear. This speed is non-dimensional, height being normalized by h_0, horizontal lengths by ℓ_c and time by $\eta\ell_c^4/(\gamma h_0^3)$.

In our experiments, using $h_+ \sim 1$, $h_d \sim 2$, we reach $v \sim 10^{-5}\,\mathrm{m\,s^{-1}}$, i.e. a speed compatible whit that measured for the domes with the highest mobility in Figure 3. We also observe that the domes with the greatest mobility move away from the wake they form. This behavior is consistent with the translation mechanism proposed by Lister *et al.* [41], with domes migration in the opposite direction to the trailing wake. However, in the the present experiment, the ratio of dome height to film thickness is of the order of one. This suggest that the addition of particles lowers the criterion to observe this mobility. Again, for pure fluid or suspension of small particles, a dome mobility around their initial growth spot is observed but does not compromise their organization into a hexagonal pattern. On the contrary, for largest particle, this organization is lost from the very beginning of their frustrated growth, resulting in the trajectories presented in Fig.3(a).

To conclude, we reported here the Rayleigh-Taylor instability of viscous thin films made of pure liquids and granular suspensions. Through interface height reconstructions, we analyzed the instability pattern and its dynamic, varying particle size relatively to the film thickness. Our findings show that when particles are significantly smaller than the film thickness, the suspension behaves similarly to a pure fluid, both in terms of pattern dimensions and structure, as well as the dynamics. In particular, in this regime, the hexagonal pattern selection remains robust. Also, the bulk suspension viscosity accurately predicts the typical growth time of the instability.

However, the behavior changes drastically for larger particles. A notable difference lies in the spatial organization of the domes, which are fewer, less organized, and exhibit significant translational motion. This motion can be attributed to frustrated growth, through volume exclusion effects, as the particles resist fluid drainage near the ceiling of the film. The motion then allows the domes to accumulate more fluid, ultimately leading to dripping.

* matthieu.roche@u-paris.fr

[1] L. Rayleigh, Investigation of the character of the equilibrium of an incompressible heavy fluid of variable density, Proceedings of the London mathematical society **1**, 170 (1882).

[2] G. I. Taylor, The instability of liquid surfaces when accelerated in a direction perpendicular to their planes. I, Proc. Royal Soc. A **201**, 192 (1950).

[3] F. Charru, *Hydrodynamic Instabilities*, 1st ed. (Cambridge University Press, Cambridge, 2011) pages: 53-67.

[4] D. H. Sharp, An overview of Rayleigh-Taylor instability, Physica D **12**, 3 (1984).

[5] D. L. Turcotte and G. Schubert, *Geodynamics*, 3rd ed. (Cambridge University Press, Cambridge, United Kingdom, 2014).

[6] J. Marthelot, E. F. Strong, M. Reis, and P.-T. Brun, Designing soft materials with interfacial instabilities in liquid films, Nature Comm. **9**, 4477 (2018).

[7] Y. Zhou, J. D. Sadler, and O. A. Hurricane, Instabilities and Mixing in Inertial Confinement Fusion, Annu. Rev. Fluid Mech. **57**, 197 (2024).

[8] C. Völtz, W. Pesch, and I. Rehberg, Rayleigh-Taylor instability in a sedimenting suspension, Phys. Rev. E **65**, 011404 (2001).

[9] J. L. Vinningland, Johnsen, E. G. Flekkøy, R. Toussaint, and K. J. Måløy, Granular Rayleigh-Taylor Instability: Experiments and Simulations, Phys. Rev. Lett. **99**, 048001 (2007).

[10] K. A. Baldwin, M. M. Scase, and R. J. A. Hill, The Inhibition of the Rayleigh-Taylor Instability by Rotation, Sci Rep **5**, 11706 (2015).

[11] G. H. Wolf, The dynamic stabilization of the Rayleigh-Taylor instability and the corresponding dynamic equilibrium, Zeitschrift für Physik A Hadrons and nuclei **227**, 291 (1969).

[12] E. Talib and A. Juel, Instability of a viscous interface under horizontal oscillation, Phys. Fluids **19**, 092102 (2007).

[13] A. J. Babchin, A. L. Frenkel, B. G. Levich, and G. I. Sivashinsky, Nonlinear saturation of Rayleigh–Taylor instability in thin films, Phys. Fluids **26**, 3159 (1983).

[14] A. Indeikina, I. Veretennikov, and H.-C. Chang, Drop fall-off from pendent rivulets, J. Fluid Mech. **338**, 173 (1997).

[15] P.-T. Brun, A. Damiano, P. Rieu, G. Balestra, and F. Gallaire, Rayleigh-Taylor instability under an inclined plane, Phys. Fluids **27**, 084107 (2015).

[16] P. H. Trinh, H. Kim, N. Hammoud, P. D. Howell, J. S. Chapman, and H. A. Stone, Curvature suppresses the Rayleigh-Taylor instability, Phys. Fluids **26**, 051704 (2014).

[17] G. Balestra, N. Kofman, P.-T. Brun, B. Scheid, and F. Gallaire, Three-dimensional Rayleigh–Taylor instability under a unidirectional curved substrate, J. Fluid Mech. **837**, 19 (2018).

[18] J. M. Burgess, A. Juel, W. D. McCormick, J. B. Swift, and H. L. Swinney, Suppression of dripping from a ceiling, Phys. Rev. Lett. **86**, 1203 (2001).

[19] S. Alqatari, T. E. Videbæk, S. R. Nagel, A. E. Hosoi, and I. Bischofberger, Confinement-induced stabilization of the Rayleigh-Taylor instability and transition to the unconfined limit, Science Advances **6**, eabd6605 (2020).

[20] M. Fermigier, L. Limat, E. Wesfreid, P. Boudinet, and C. Quilliet, Two-dimensional patterns in Rayleigh-Taylor instability of a thin layer, J. Fluid Mech. **236**, 349 (1992).

[21] H.-J. Kull, Theory of the rayleigh-taylor instability, Physics Reports **206**, 197 (1991).

[22] W. Harrison, XLIX. On the stability of superposed streams of viscous liquids, The London, Edinburgh, and Dublin Philosophical Magazine and Journal of Science **20**, 493 (1910).

[23] R. Bellman and R. H. Pennington, Effects of surface tension and viscosity on Taylor instability, Quarterly of Applied Mathematics **12**, 151 (1954).

[24] R. Menikoff, R. C. Mjolsness, D. H. Sharp, and C. Zemach, Unstable normal mode for Rayleigh–Taylor instability in viscous fluids, The Physics of Fluids **20**, 2000.

[25] M. Fermigier, L. Limat, E. Wesfreid, P. Boudinet, C. Ghidaglia, and C. Quilliet, Rayleigh-Taylor instability of a thin layer, Growth and Form: Nonlinear Aspects , 441 (1991).

[26] L. Limat, P. Jenffer, B. Dagens, E. Touron, M. Fermigier, and J. Wesfreid, Gravitational instabilities of thin liquid layers: dynamics of pattern selection, Physica D **61**, 166 (1992).

[27] Guazzelli and O. Pouliquen, Rheology of dense granular suspensions, J. Fluid Mech. **852**, P1 (2018).

[28] S. Wildeman, Real-time quantitative Schlieren imaging by fast Fourier demodulation of a checkered backdrop, Exp. Fluids **59**, 97 (2018).

[29] A. Gans, E. Dressaire, B. Colnet, G. Saingier, M. Z. Bazant, and A. Sauret, Dip-coating of suspensions, Soft matter **15**, 252 (2019).

[30] S. Palma and H. Lhuissier, Dip-coating with a particulate suspension, J. Fluid Mech. **869**, R3 (2019).

[31] A. Sauret, A. Gans, B. Colnet, G. Saingier, M. Z. Bazant, and E. Dressaire, Capillary filtering of particles during dip coating, Phys. Rev. Fluids **4**, 054303 (2019).

[32] D.-H. Jeong, M. K. H. Lee, V. Thiévenaz, M. Z. Bazant, and A. Sauret, Dip coating of bidisperse particulate suspensions, J. Fluid Mech. **936** (2022).

[33] J. Château, Guazzelli, and H. Lhuissier, Pinch-off of a viscous suspension thread, J. Fluid Mech. **852**, 178 (2018).

[34] J. Château and H. Lhuissier, Breakup of a particulate suspension jet, Phys. Rev. Fluids **4**, 012001 (2019).

[35] M. Zhao, M. Oléron, A. Pelosse, L. Limat, Guazzelli, and M. Roché, Spreading of granular suspensions on a solid surface, Phys. Rev. Research **2**, 022031 (2020).

[36] A. Pelosse, Guazzelli, and M. Roché, Probing dissipation in spreading drops with granular suspensions, J. Fluid Mech. **955**, A7 (2023).

[37] E. Pitts, The stability of pendent liquid drops. Part 2. Axial symmetry, J. Fluid Mech. **63**, 487 (1974).

[38] A. Myshkis, V. Babskii, N. Kopachevskii, L. Slobozhanin, A. Tyuptsov, and R. Wadhwa, *Low-gravity fluid mechanics, mathematical theory of capillary phenomena* (Springer-Verlag, 1987) pages: 152-154.

[39] P. T. Sumesh and R. Govindarajan, The possible equilibrium shapes of static pendant drops, J. Chem. Phys. **133**, 144707 (2010).

[40] S. G. Yiantsios and B. G. Higgins, Rayleigh–Taylor instability in thin viscous films, Phys. Fluids A **1**, 1484 (1989).

[41] J. R. Lister, J. M. Rallison, and S. J. Rees, The nonlinear dynamics of pendent drops on a thin film coating the underside of a ceiling, J. Fluid Mech. **647**, 239 (2010).

End Matter

Materials

Transparent suspensions are made of PMMA spheres (Spheromers CA, Microbeads, or Altuglas, Arkema) immersed in a mixture of Triton X-100 (73 wt%), zinc chloride (16 wt%), and water (11 wt%) matching the density and optical index of PMMA. Additional opaque suspensions are made of spherical polystyrene beads (Dynoseeds TS, Microbeads, Norway) suspended in a density-matched Newtonian PEG copolymer [Poly(ethylene glycol-ran-propylene glycol) monobutyl ether] (Sigma). The dynamic viscosity of the two suspending fluid are $\eta_f = (3.3 \pm 0.1)\,\mathrm{Pa\,s}$ and $(2.4 \pm 0.1)\,\mathrm{Pa\,s}$ at 22 °C, and their surface tension $\gamma_f \simeq 32$ and $35\,\mathrm{mN\,m^{-1}}$, respectively. On a une idée des viscosités des suspensions? On les a mesurés quelque part? The surface tension of the suspensions is that of the suspending fluid, as confirmed by pendant drop experiments. PMMA particle diameters are $(60 \pm 6)\,\mu\mathrm{m}$, $(220 \pm 10)\,\mu\mathrm{m}$, $(265 \pm 15)\,\mu\mathrm{m}$ and $(325 \pm 10)\,\mu\mathrm{m}$ and polystyrene particle diameters are $(80 \pm 6)\,\mu\mathrm{m}$, $(140 \pm 10)\,\mu\mathrm{m}$ and $(250 \pm 15)\,\mu\mathrm{m}$. The suspension mixture is made by weighting a mass of suspending fluid, adding the amount of solid needed to reach the desired particle volume fraction $\phi = 30\,\%$. Regular, slow machine mixing ensures homogenization and removal of air bubbles. The particles are found to be completely wet by the fluid and to experience no aggregation.

Film Preparation

Thin films are prepared on a glass plate on which a plastic frame of thickness $h_0 = 500$ or $750\,\mu\mathrm{m}$ is glued. The plate is placed on a scale, and the desired mass of fluid is slowly poured homogeneously in the frame and left to rest for several hours before an experiment. Once turned over, the fluid does not wet the plastic sufficiently to spread on it. The instability always starts from the edges and propagates to the center. For this reason, the frame is cut with a hexagonal shape (side length 9 cm), to generate directly the most unstable lattice of domes.

Surface Profilometry

The total apparatus is a 1-meter high structure holding a LED panel placed above the glass plate, which is itself above a mirror, inclined at 45° to image from below. As drops drip on the mirror, the field of view shrinks during an experiment. The acquisition is made with a monochrome Basler camera (reference acA12440 - 35 um, 5 MP) mounted with a distortionless macro lens (reference VS-LLD30). The typical resolution is 130 µm/pixel and the distance between the camera and the liquid film is $H = 1.1\,\mathrm{m}$. A checkerboard in which each square has a side length 1 mm is printed on a paper sheet and taped

on the other side of the glass plate and can be used for visualization and in particular for Synthetic Schlieren Imaging. The latter technique can be used with transparent suspensions, as the checkerboard pattern can be seen through and appears distorted by the deformed interface. Such pictures can be quickly inverted through Fourier demodulation, enabling non-invasive surface profilometry of the free interface [**?**].

Thin-film analysis of the RTI

A simple yet informative treatment of the RTI considers a thin layer of viscous liquid of initial thickness h_0 that hangs from a rigid ceiling into another fluid. The system is assumed infinite in all other directions. The dynamic viscosity η and density ρ of the liquid are assumed to be much larger than that of the ambient fluid. The surface tension of the liquid with air is γ. Under the lubrication approximation, the spatiotemporal evolution of the film thickness h follows [**?**],

$$\frac{\partial h}{\partial t} + \nabla \cdot \left[\frac{h^3}{3\eta} \nabla \left(\rho g h + \gamma \Delta h \right) \right] = 0, \tag{3}$$

with ∇ and Δ the in-plane gradient and Laplacian operators, respectively, g, the acceleration of gravity with $g > 0$, such that the vertical direction is directed downwards and normal to the solid surface located at $z = 0$. Assuming that $h = h_0 + \delta h$ with $\delta h(x,y,t) << h_0$ the interface displacement, Eq. 3 can be linearized.

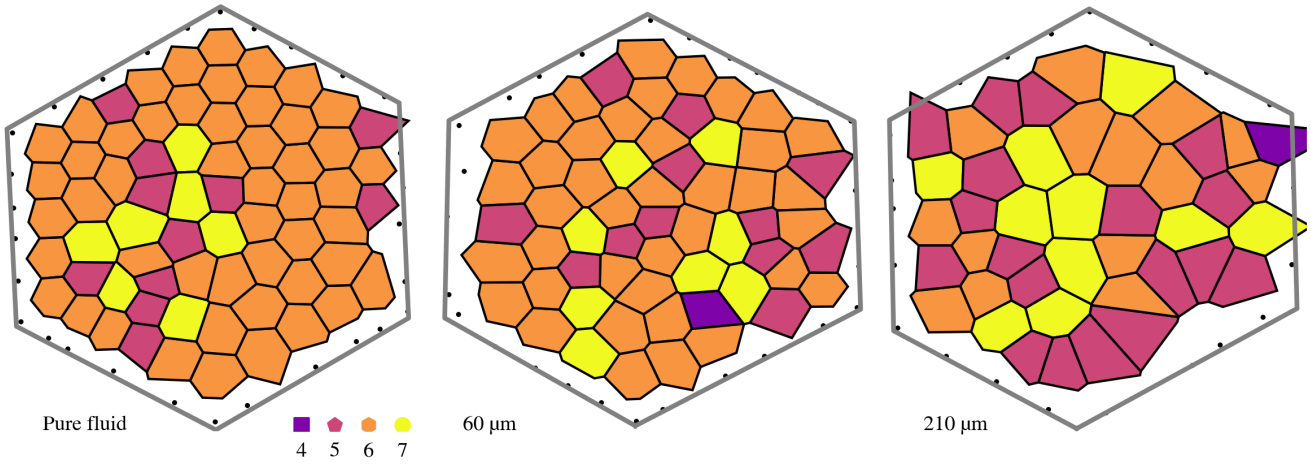
Pure fluid
4
5
6
7
60 µm
210 µm